

Fourth order summation-by-parts finite difference methods for 3-D elastic wave propagation in curvilinear coordinates with mesh refinement interfaces

Lu Zhang Siyang Wang N. Anders Petersson

January 13, 2020

Abstract

We develop a fourth order finite difference method for the three-dimensional elastic wave equation in anisotropic media with piecewise smooth material property. In our model, the material property can be discontinuous at curved interfaces. The governing equations are discretized in second order form on curvilinear meshes by using a fourth order finite difference operator satisfying a summation-by-parts property. A highlight of our method is that mesh sizes can be chosen according to the velocity structure of the material so that computational efficiency is improved. At mesh refinement interfaces with hanging nodes, physical interface conditions are imposed by using ghost points and interpolation. We prove energy stability of the discretization. With a fourth order predictor-corrector time integrator, the fully discrete scheme is energy conserving. Numerical experiments are presented to verify the fourth order convergence rate, and the energy conserving property.

1 Introduction

Seismic wave propagation has important applications in earthquake simulation and forecasting, energy resources exploration, and underground motion analysis. In many practical problems, the wave motion is governed by the three dimensional (3D) anisotropic elastic wave equations. The layered structure of the Earth gives rise to a piecewise smooth material property with discontinuities at internal interfaces, which are often curved in realistic models. At an interface between two elastic media, wave interaction can create a so-called Stonely wave that propagates along the interface and decays exponentially away from the interface. Because of the heterogeneous material property and internal interfaces, the governing equations cannot be solved analytically, and it is necessary to use advanced numerical techniques to solve the seismic wave propagation problems.

When solving hyperbolic partial differential equations (PDEs), for computational efficiency, it is essential that the numerical methods are high order accurate (fourth order or higher). This is because high order methods have much smaller dispersion error than lower order methods, see the analysis of dispersion relation for first order hyperbolic PDEs [3] and second order hyperbolic PDEs [2]. However, it is challenging to obtain high order accuracy in the presence of discontinuous material property and non-trivial geometry.

Traditionally, the governing equations of seismic wave propagation are solved as a first order system, either in velocity-strain or velocity-stress formulation, which consists of nine equations. The first order system can be solved by the well-known numerical methods developed in the computational fluid dynamics community. (ADD Some recent works for first order systems)

In this paper, we use another approach that discretizes the governing equations in second order form. Comparing with nine PDEs in a first order system, the second order form consists of only three PDEs in the displacement variables. In many cases, this could be a more efficient approach in terms of accuracy and memory usage. For spatial discretization, we consider the finite difference operators constructed in [6] that satisfy a summation-by-parts (SBP) principle. The SBP is a discrete analogue of the integration-by-parts, and is an important ingredient to obtain energy stability.

In the SBP finite difference framework, a multi-block approach is often taken when the material property is discontinuous. That is, the domain is divided into subdomains such that the internal interfaces are aligned with the material discontinuities. SBP operators are then used independently in each subdomain for the spatial discretization of the governing equation. To patch subdomains together, physical interface conditions are imposed at internal interfaces.

In [5], a fourth order SBP finite difference method is developed to solve the 3D elastic wave equation in heterogeneous smooth media, where topography in non-rectangular domains is resolved by using curvilinear meshes. The main objective of the present paper is to develop a fourth order method that solves the governing equations in piecewise smooth media where material discontinuities occur at curved interfaces. This is motivated by the fact that in realistic models, material properties are only piecewise smooth with discontinuities, and it is important to obtain high order accuracy even at the material interfaces. A highlight of our method is that mesh sizes in each subdomain can be chosen according to the velocity structure of the material property so that computational efficiency is maximized. More precisely, as going deeper in the Earth, the wave speed gets larger and the wavelength gets longer. Correspondingly, in our model, the mesh becomes coarser from one subdomain to the next one underneath. In this way, the number of grid points per wavelength can be kept almost the same in the entire domain.

For mesh refinement interfaces, we have constructed fourth order interpolation and restriction operators to impose the interface conditions at the hanging nodes. These operators are compatible with the underlying SBP operators. With a fourth order predictor-corrector time integrator, the fully discrete discretization is energy conserving.

The rest of the paper is organized as follows. In Sec. 2, we introduce the governing equation in curvilinear coordinates. The spatial discretization is presented in detail in Sec. 3. Particular emphasize is placed on the numerical coupling procedure at curved mesh refinement interfaces. In Sec. 4, we describe the temporal discretization, and present the fully discrete scheme. Numerical experiments are presented in Sec. 5 to verify the convergence rate of the proposed scheme and the energy conserving property. We also demonstrate that the mesh refinement interfaces do not introduce spurious wave reflections. In the end, we draw conclusion in Sec. 6.

2 The isotropic elastic wave equation

We consider the time dependent isotropic elastic wave equation in three dimensions. The problem is defined on a curvilinear domain $\mathbf{x} \in \Omega$, $\mathbf{x} = (x^1, x^2, x^3)^T$ with a mesh refinement interface Γ . We partition the domain Ω into two subdomains Ω^f and Ω^c such that the interface Γ is aligned with a subdomain boundary with $\Omega = \Omega^f \cup \Omega^c$ and $\Gamma = \Omega^f \cap \Omega^c$. Denote $\mathbf{F} = (F_1, F_2, F_3)^T$ to be the three dimensional displacement vector on Ω^f and $\mathbf{C} = (C_1, C_2, C_3)^T$ to be the three dimensional displacement vector on Ω^c . By introducing smooth one-to-one mapping

$$\mathbf{x}^f = \mathbf{X}^f(\mathbf{r}) : \Omega_r^f = [0, 1]^3 \rightarrow \Omega^f \subset \mathbb{R}^3$$

with $\mathbf{X}^f(\mathbf{r}) = (x^{f,1}(\mathbf{r}), x^{f,2}(\mathbf{r}), x^{f,3}(\mathbf{r}))^T$, $\mathbf{r} = (r^1, r^2, r^3)^T$, $0 \leq r^i \leq 1$, $i = 1, 2, 3$ and one-to-one mapping

$$\mathbf{x}^c = \mathbf{X}^c(\mathbf{r}) : \Omega_r^c = [0, 1]^3 \rightarrow \Omega^c \subset \mathbb{R}^3$$

with $\mathbf{X}^c(\mathbf{r}) = (x^{c,1}(\mathbf{r}), x^{c,2}(\mathbf{r}), x^{c,3}(\mathbf{r}))^T$, $\mathbf{r} = (r^1, r^2, r^3)^T$, $0 \leq r^i \leq 1$, $i = 1, 2, 3$. Note that $\Omega_r^f = \Omega_r^c$. To have a better understanding, we refer Figure 2 as an illustration. Indeed, we want to mention that the interface Γ corresponds to $r^3 = 1$ for coarse domain and $r^3 = 0$ for fine domain, that is we assume the fine domain Ω^f is on the top of coarse domain Ω^c in this paper. Then the elastic wave equation can be written in curvilinear coordinates as

$$\begin{aligned} \rho^f \frac{\partial^2 \mathbf{F}}{\partial^2 t} &= \frac{1}{J^f} \left[\partial_1(A_1^f \nabla \mathbf{F}) + \partial_2(A_2^f \nabla \mathbf{F}) + \partial_3(A_3^f \nabla \mathbf{F}) \right], \quad \mathbf{r} \in \Omega_r^f, \quad t \geq 0, \\ \rho^c \frac{\partial^2 \mathbf{C}}{\partial^2 t} &= \frac{1}{J^c} [\partial_1(A_1^c \nabla \mathbf{C}) + \partial_2(A_2^c \nabla \mathbf{C}) + \partial_3(A_3^c \nabla \mathbf{C})], \quad \mathbf{r} \in \Omega_r^c, \quad t \geq 0, \end{aligned} \quad (1)$$

where ρ^f and ρ^c are density functions for fine domain Ω^f and coarse domain Ω^c respectively, and $\partial_i = \frac{\partial}{\partial r_i}$, $\nabla = (\partial_1, \partial_2, \partial_3)$. For the rest of paper, we introduce a notation $\{\cdot, \cdot\}$ which represents the componentwise identities, then

$$\begin{aligned} A_1^{\{f,c\}} \nabla \{\mathbf{F}, \mathbf{C}\} &:= N_{11}^{\{f,c\}} \partial_1 \{\mathbf{F}, \mathbf{C}\} + N_{12}^{\{f,c\}} \partial_2 \{\mathbf{F}, \mathbf{C}\} + N_{13}^{\{f,c\}} \partial_3 \{\mathbf{F}, \mathbf{C}\}, \\ A_2^{\{f,c\}} \nabla \{\mathbf{F}, \mathbf{C}\} &:= N_{21}^{\{f,c\}} \partial_1 \{\mathbf{F}, \mathbf{C}\} + N_{22}^{\{f,c\}} \partial_2 \{\mathbf{F}, \mathbf{C}\} + N_{23}^{\{f,c\}} \partial_3 \{\mathbf{F}, \mathbf{C}\}, \\ A_3^{\{f,c\}} \nabla \{\mathbf{F}, \mathbf{C}\} &:= N_{31}^{\{f,c\}} \partial_1 \{\mathbf{F}, \mathbf{C}\} + N_{32}^{\{f,c\}} \partial_2 \{\mathbf{F}, \mathbf{C}\} + N_{33}^{\{f,c\}} \partial_3 \{\mathbf{F}, \mathbf{C}\}, \end{aligned}$$

with

$$N_{ij}^{\{f,c\}} = J^{\{f,c\}} (P_i^{\{f,c\}})^T M^{\{f,c\}} P_j^{\{f,c\}}.$$

Here, $M^{\{f,c\}}$ are 6×6 stiffness matrices and they are symmetric and positive definite. Especially, for isotropic elastic wave equation, we have

$$\begin{aligned} M_{11}^{\{f,c\}} &= \begin{pmatrix} 2\mu^{\{f,c\}} + \lambda^{\{f,c\}} & 0 & 0 \\ 0 & \mu^{\{f,c\}} & 0 \\ 0 & 0 & \mu^{\{f,c\}} \end{pmatrix}, \quad M_{12}^{\{f,c\}} = \begin{pmatrix} 0 & \lambda^{\{f,c\}} & 0 \\ \mu^{\{f,c\}} & 0 & 0 \\ 0 & 0 & 0 \end{pmatrix}, \\ M_{22}^{\{f,c\}} &= \begin{pmatrix} \mu^{\{f,c\}} & 0 & 0 \\ 0 & 2\mu^{\{f,c\}} + \lambda^{\{f,c\}} & 0 \\ 0 & 0 & \mu^{\{f,c\}} \end{pmatrix}, \quad M_{13}^{\{f,c\}} = \begin{pmatrix} 0 & 0 & \lambda^{\{f,c\}} \\ 0 & 0 & 0 \\ \mu^{\{f,c\}} & 0 & 0 \end{pmatrix}, \\ M_{33}^{\{f,c\}} &= \begin{pmatrix} \mu^{\{f,c\}} & 0 & \lambda^{\{f,c\}} \\ 0 & \mu^{\{f,c\}} & 0 \\ 0 & 0 & 2\mu^{\{f,c\}} + \lambda^{\{f,c\}} \end{pmatrix}, \quad M_{23}^{\{f,c\}} = \begin{pmatrix} 0 & 0 & 0 \\ 0 & 0 & \lambda^{\{f,c\}} \\ 0 & \mu^{\{f,c\}} & 0 \end{pmatrix}, \\ M_{31}^{\{f,c\}} &= (M_{13}^{\{f,c\}})^T, \quad M_{32}^{\{f,c\}} = (M_{23}^{\{f,c\}})^T, \quad M_{21}^{\{f,c\}} = (M_{12}^{\{f,c\}})^T. \end{aligned} \quad (2)$$

Here, $\lambda^{\{f,c\}}$ and $\mu^{\{f,c\}}$ are the first and second Láme parameters respectively, which are determined by the properties of the materials. We refer to Appendix A for the definitions of matrices $P_i^{\{f,c\}}$, $i = 1, 2, 3$. From the definitions of matrices $N_{ij}^{\{f,c\}}$, we have that $N_{ii}^{\{f,c\}}$, $i = 1, 2, 3$, are symmetric positive definite, and $N_{ij}^{\{f,c\}} = (N_{ji}^{\{f,c\}})^T$, $i, j = 1, 2, 3$. The Jacobian of transformation is $J^{\{f,c\}} = \det(\mathbf{a}_1^{\{f,c\}}, \mathbf{a}_2^{\{f,c\}}, \mathbf{a}_3^{\{f,c\}})$, $0 < J^{\{f,c\}} < \infty$, with the derivative of the forward mapping,

$$\mathbf{a}_k^{\{f,c\}} := \partial_k \mathbf{x}^{\{f,c\}} = \left(\frac{\partial x^{\{f,c\},1}}{\partial r^k}, \frac{\partial x^{\{f,c\},2}}{\partial r^k}, \frac{\partial x^{\{f,c\},3}}{\partial r^k} \right)^T, \quad k = 1, 2, 3,$$

and the backward mapping,

$$\mathbf{a}^{\{f,c\},k} := \nabla_x^{\{f,c\}} r^k = \left(\frac{\partial r^k}{\partial x^{\{f,c\},1}}, \frac{\partial r^k}{\partial x^{\{f,c\},2}}, \frac{\partial r^k}{\partial x^{\{f,c\},3}} \right)^T := \left(\xi_{1k}^{\{f,c\}}, \xi_{2k}^{\{f,c\}}, \xi_{3k}^{\{f,c\}} \right)^T, \quad k = 1, 2, 3.$$

The metric relation is given by [7],

$$\mathbf{a}^{\{f,c\},i} = \frac{1}{J^{\{f,c\}}} \left(\mathbf{a}_j^{\{f,c\}} \times \mathbf{a}_k^{\{f,c\}} \right), \quad (i, j, k) \text{ cycle.}$$

Denote the unit outward normal $\mathbf{n}_i^{\{f,c\},\pm} = (n_i^{\{f,c\},\pm,1}, n_i^{\{f,c\},\pm,2}, n_i^{\{f,c\},\pm,3})$, $i = 1, 2, 3$, for the boundaries of i 'th direction on subdomain $\Omega^{\{f,c\}}$, then

$$\begin{aligned} \mathbf{n}_i^{\{f,c\},\pm} &:= (n_i^{\{f,c\},\pm,1}, n_i^{\{f,c\},\pm,2}, n_i^{\{f,c\},\pm,3})^T = \pm \frac{\nabla_x^{\{f,c\}} r^i}{|\nabla_x^{\{f,c\}} r^i|} \\ &= \pm \frac{\left(\xi_{1i}^{\{f,c\}}, \xi_{2i}^{\{f,c\}}, \xi_{3i}^{\{f,c\}} \right)^T}{\sqrt{(\xi_{1i}^{\{f,c\}})^2 + (\xi_{2i}^{\{f,c\}})^2 + (\xi_{3i}^{\{f,c\}})^2}}, \end{aligned} \quad (3)$$

here, '+' corresponds to $r^i = 1$ and '-' corresponds to $r^i = 0$. At the interface Γ , the traction vectors and displacement vectors are continuous with

$$\frac{A_3^f \nabla \mathbf{F}}{J^f |\nabla_x^f r^3|} = \frac{A_3^c \nabla \mathbf{C}}{J^c |\nabla_x^c r^3|}, \quad \mathbf{F} = \mathbf{C}. \quad (4)$$

By ignoring physical boundaries and combining with (4), then we can prove the problem is well-posed with a similar analysis as in [1, 5].

3 The spatial discretization

In this section, we describe the spatial discretization for the problem (1). We firstly introduce the SBP operator for the first and second spatial derivative with scalar variable in one dimension and then extend the SBP operators to vector variables in three dimensions.

3.1 SBP operators in 1D

Consider a uniform discretization of the domain $x \in [0, 1]$ with the grids,

$$\tilde{\mathbf{x}} = [x_0, x_1, \dots, x_n, x_{n+1}]^T, \quad x_i = (i-1)h, \quad i = 0, 1, \dots, n, n+1, \quad h = 1/(n-1),$$

where $i = 1, n$ correspond to the grid points on the boundary, and $i = 0, n+1$ are ghost points outside of the physical domain. The operator $D \approx \frac{\partial}{\partial x}$ is a first derivative SBP operator if

$$(\mathbf{u}, D\mathbf{v})_h = -(D\mathbf{u}, \mathbf{v})_h - u_1 v_1 + u_n v_n, \quad (5)$$

with a scalar product

$$(\mathbf{u}, \mathbf{v})_h = h \sum_{i=1}^n \omega_i u_i v_i. \quad (6)$$

Here, $0 < \omega_i < \infty$ are the weights of scalar product. The SBP operator D has a centered difference stencil at the grid points away from the boundary and the corresponding weights $\omega_i = 1$. To satisfy the SBP identity (5), the coefficients in D are modified at a few points near the boundary and the corresponding weights $\omega_i \neq 1$. The operator D does not use any ghost points. Similarly, we can define another operator $\tilde{D} \approx \frac{\partial}{\partial x}$ which uses one ghost point outside each boundary as

$$(\mathbf{u}, \tilde{D}\mathbf{v})_h = -(D\mathbf{u}, \mathbf{v})_h - u_1 v_1 + u_n v_n. \quad (7)$$

To discretize the elastic wave equation, we also need to approximate the second derivative with variable coefficient $(\gamma(x)u_x)_x$. Here, the known function $\gamma(x) > 0$ describes the property of the material. There are two different fourth order accurate SBP operators for the approximation of $(\gamma(x)u_x)_x$. The first one $\tilde{G}(\gamma)\mathbf{u} \approx (\gamma(x)u_x)_x$, derived by Sjögreen and Petersson [6], uses one ghost point outside each boundary, and satisfies the second derivative SBP identity,

$$(\mathbf{u}, \tilde{G}(\gamma)\mathbf{v})_h = -P_\gamma(\mathbf{u}, \mathbf{v}) - u_1 \gamma_1 \tilde{\mathbf{b}}_1 \mathbf{v} + u_n \gamma_n \tilde{\mathbf{b}}_n \mathbf{v}. \quad (8)$$

Here, the bilinear form $P_\gamma(\cdot, \cdot)$ is symmetric and positive semi-definite, and does not use any ghost points. The operators $\tilde{\mathbf{b}}_1$ and $\tilde{\mathbf{b}}_n$ approximate the first derivative on the left and right boundaries, respectively. Using the left boundary as an example, we have

$$\tilde{\mathbf{b}}_1 \mathbf{v} = \frac{1}{h} \sum_{i=0}^4 d_i v_i, \quad (9)$$

as the fourth order accurate approximation of $u_x(x_1)$. We note that the notation $\tilde{G}(\gamma)\mathbf{v}$ implies that the operator \tilde{G} uses \mathbf{v} on all grid points $\tilde{\mathbf{x}}$, but $\tilde{G}(\gamma)\mathbf{v}$ only returns values on the grid \mathbf{x} without ghost points. Therefore, when writing in matrix form, \tilde{G} is a non-square matrix of size n by $n+2$.

The other SBP operator $G(\gamma)\mathbf{u} \approx (\gamma(x)u_x)_x$ is developed by Mattsson [4] without using any ghost points, and satisfies a similar SBP identity,

$$(\mathbf{u}, G(\gamma)\mathbf{v})_h = -P_\gamma(\mathbf{u}, \mathbf{v}) - u_1 \gamma_1 \mathbf{b}_1 \mathbf{v} + u_n \gamma_n \mathbf{b}_n \mathbf{v}. \quad (10)$$

Here, \mathbf{b}_1 and \mathbf{b}_n are also finite difference operators for the first derivative at the boundaries, but are constructed to third order accurate,

$$\mathbf{b}_1 \mathbf{v} = \frac{1}{h} \sum_{i=1}^4 d_i v_i. \quad (11)$$

In this case, $G(\gamma)$ is square in matrix form.

For the second derivative SBP operators $\tilde{G}(\gamma)$ and $G(\gamma)$, both of them use a fourth order five points centered difference stencil to approximate $(\gamma u_x)_x$ on the interior points away from the boundaries. For the first and the last six grid points close to the boundaries, the operators $G(\gamma)$ and $\tilde{G}(\gamma)$ use second order accurate one-sided difference stencils. They are designed to satisfy (10) and (8), respectively. In the following sections, we use both of them to develop a multi-block finite difference discretization for the elastic wave equation.

3.2 Semi-discretization of the elastic wave equation

In this section, we discretize the elastic wave equation (1) with mesh refinement interface Γ . Without losing generality, we assume the ratio of mesh sizes for subdomain Ω_r^f and subdomain Ω_r^c is $1 : 2$, that is the mesh sizes of Ω_r^f and Ω_r^c satisfy

$$h_1(n_1^h - 1) = 1, \quad h_2(n_2^h - 1) = 1, \quad h_3(n_3^h - 1) = 1$$

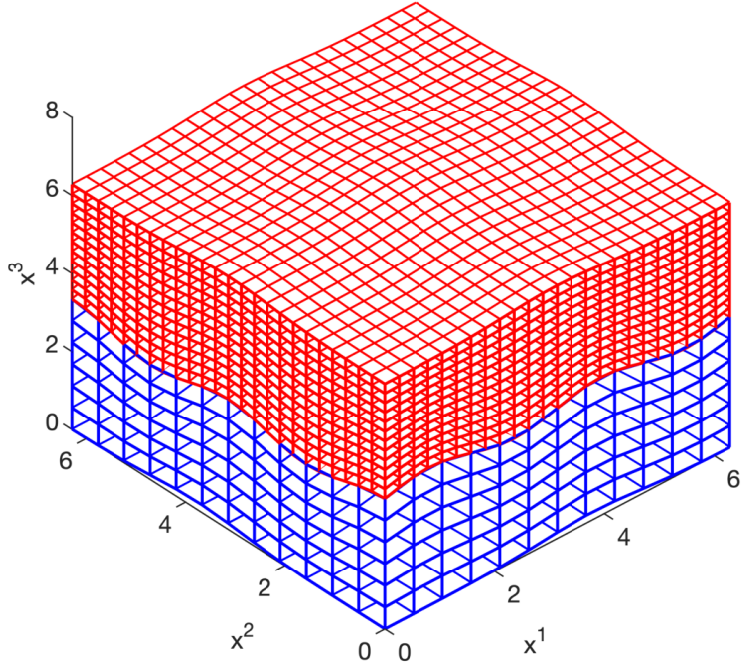


Figure 1: The sketch for the spatial discretization of physical domain Ω . The blue region is the spacial discretization of coarse subdomain Ω^c and the red region is the spatial discretization of fine domain Ω^f .

and

$$2h_1(n_1^{2h} - 1) = 1, \quad 2h_2(n_2^{2h} - 1) = 1, \quad 2h_3(n_3^{2h} - 1) = 1$$

respectively, other ratios can be treated analogously. Figure 1 gives an illustration of the discretization of a physical domain.

We focus on the numerical treatment of the interface conditions (4) and suppose boundaries are periodic in directions 1 and 2, ignore the boundaries in direction 3. In Figure 2, we fix $x^2 = 0$ and present the x^1 - x^3 section of the domain Ω . To condense notations, we introduce the multi-index notations

$$\mathbf{i} = (i, j, k), \quad \mathbf{r}_i = (r_i^1, r_j^2, r_k^3), \quad \mathbf{x}_i^{\{f,c\}} = (x_i^{\{f,c\},1}, x_j^{\{f,c\},2}, x_k^{\{f,c\},3}), \quad \mathbf{x}_i^{\{f,c\}} = \mathbf{X}^{\{f,c\}}(\mathbf{r}_i).$$

Note that for $\mathbf{x}_i^f \in \Omega^f$, we have $i \in [1, n_1^h]$, $j \in [1, n_2^h]$, $k \in [1, n_3^h]$; for $\mathbf{x}_i^c \in \Omega^c$, we have $i \in [1, n_1^{2h}]$, $j \in [1, n_2^{2h}]$, $k \in [1, n_3^{2h}]$; for $\mathbf{x}_i^c \in \Gamma \cap \Omega^c := \Gamma^c$, we have $i \in [1, n_1^{2h}]$, $j \in [1, n_2^{2h}]$, $k = n_3^{2h}$; for $\mathbf{x}_i^f \in \Gamma \cap \Omega^f := \Gamma^f$, we have $i \in [1, n_1^h]$, $j \in [1, n_2^h]$, $k = 1$; for $\mathbf{x}_i^f \in \Omega^f \setminus \Gamma := \overline{\Gamma^f}$, we have $i \in [1, n_1^h]$, $j \in [1, n_2^h]$, $k \in [2, n_3^h]$. Now, denote the grid functions in Ω^f and Ω^c as

$$\mathbf{f} = (\mathbf{f}^1, \mathbf{f}^2, \mathbf{f}^3)^T \quad \text{and} \quad \mathbf{c} = (\mathbf{c}^1, \mathbf{c}^2, \mathbf{c}^3)^T$$

respectively. Here,

$$\mathbf{f}^l \approx F_l(\mathbf{r}), \quad \mathbf{X}^f(\mathbf{r}) \in \Omega^f, \quad l = 1, 2, 3,$$

and

$$\mathbf{c}^l \approx C_l(\mathbf{r}), \quad \mathbf{X}^c(\mathbf{r}) \in \Omega^c \quad l = 1, 2, 3.$$

Furthermore, we define \mathbf{f}_Γ as the grid function for $\mathbf{X}^f(\mathbf{r}) \in \Gamma^f$, \mathbf{c}_Γ to be the grid function for $\mathbf{X}^c(\mathbf{r}) \in \Gamma^c$ and $\mathbf{f}_{\overline{\Gamma}}$ as the grid function for $\mathbf{X}^f(\mathbf{r}) \in \overline{\Gamma^f}$. Particularly, we define $\tilde{\mathbf{c}} = (\tilde{\mathbf{c}}^1, \tilde{\mathbf{c}}^2, \tilde{\mathbf{c}}^3)^T$ as

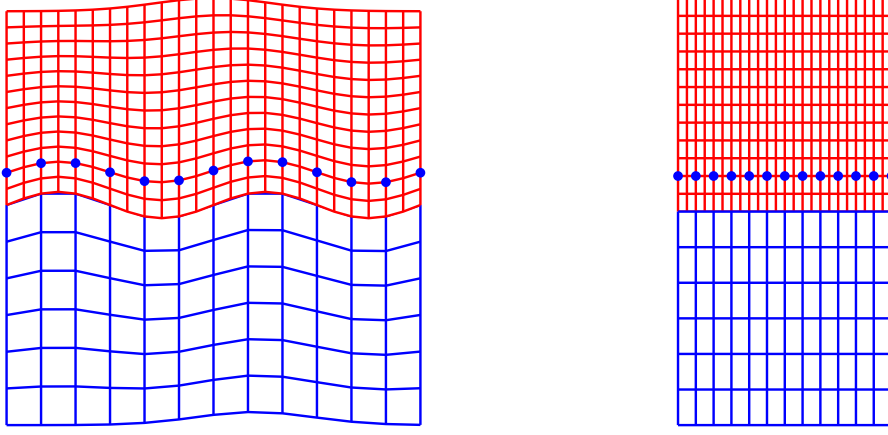


Figure 2: The sketch of spacial discretization of x^1 - x^3 section with $x^2 = 0$. From the left to the right are for physcial domain and parameter space respectively. The blue dots are the ghost points for coarse domain Ω^c .

the grid function which contain both grids in Ω^c and ghost points outside of Ω^c with $i \in [1, n_1^{2h}], j \in [1, n_2^{2h}], k \in [0, n_3^{2h} + 1]$. Then we approximate the elastic wave equation (1) on Ω^c by

$$\varrho^{2h} \mathbf{c}_{tt} = (\mathcal{J}^{2h})^{-1} \left(\sum_{l=1}^2 \mathcal{G}_l^{2h}(N_{ll}) \mathbf{c} + \tilde{\mathcal{G}}_3^{2h}(N_{33}) \tilde{\mathbf{c}} + \sum_{l=1}^3 \sum_{m=1, m \neq l}^3 \mathcal{D}_l^{2h}(\mathcal{N}_{lm}^{2h} \mathcal{D}_m^{2h} \mathbf{c}) \right) := \tilde{L}^{2h} \tilde{\mathbf{c}}, \quad (12)$$

where

$$\varrho^{2h} = \begin{pmatrix} \boldsymbol{\rho}^{2h} & & \\ & \boldsymbol{\rho}^{2h} & \\ & & \boldsymbol{\rho}^{2h} \end{pmatrix}, \quad \mathcal{J}^{2h} = \begin{pmatrix} \mathbf{J}^{2h} & & \\ & \mathbf{J}^{2h} & \\ & & \mathbf{J}^{2h} \end{pmatrix} \quad (13)$$

with both $\boldsymbol{\rho}^{2h}$ and \mathbf{J}^{2h} are $n_1^{2h} n_2^{2h} n_3^{2h} \times n_1^{2h} n_2^{2h} n_3^{2h}$ diagonal matrices with diagonal entries are values of density function ρ^c and Jacobian of transformation J^c on the grids in Ω^c respectively. And $\mathcal{G}_l^{2h}(N_{ll}), l = 1, 2$ are defined as

$$\mathcal{G}_l^{2h}(N_{ll}) = \begin{pmatrix} G_l^{2h}(N_{ll}^{11}) & G_l^{2h}(N_{ll}^{12}) & G_l^{2h}(N_{ll}^{13}) \\ G_l^{2h}(N_{ll}^{21}) & G_l^{2h}(N_{ll}^{22}) & G_l^{2h}(N_{ll}^{23}) \\ G_l^{2h}(N_{ll}^{31}) & G_l^{2h}(N_{ll}^{32}) & G_l^{2h}(N_{ll}^{33}) \end{pmatrix}, \quad (14)$$

with $G_l^{2h}(N_{ll}^{ij}), i, j = 1, 2, 3$, are $n_1^{2h} n_2^{2h} n_3^{2h} \times n_1^{2h} n_2^{2h} n_3^{2h}$ matrices which are from the central difference operator for second derivative with variable coefficient in direction l , the superscript ij represents the i 'th row and j 'th column of matrix N_{ll} . As for $\tilde{\mathcal{G}}_3^{2h}(N_{33})$, it has a structure

$$\tilde{\mathcal{G}}_3^{2h}(N_{33}) = \begin{pmatrix} \tilde{G}_3^{2h}(N_{33}^{11}) & \tilde{G}_3^{2h}(N_{33}^{12}) & \tilde{G}_3^{2h}(N_{33}^{13}) \\ \tilde{G}_3^{2h}(N_{33}^{21}) & \tilde{G}_3^{2h}(N_{33}^{22}) & \tilde{G}_3^{2h}(N_{33}^{23}) \\ \tilde{G}_3^{2h}(N_{33}^{31}) & \tilde{G}_3^{2h}(N_{33}^{32}) & \tilde{G}_3^{2h}(N_{33}^{33}) \end{pmatrix},$$

where $\tilde{G}_3^{2h}(N_{33}^{ij}), i, j = 1, 2, 3$, are $n_1^{2h} n_2^{2h} n_3^{2h} \times n_1^{2h} n_2^{2h} (n_3^{2h} + 2)$ matrices which are defined as in (8) for direction 3. Finally, let's look at the term $\mathcal{D}_l^{2h}(\mathcal{N}_{lm}^{2h} \mathcal{D}_m^{2h})$, $l = 1, 2, 3, m = 1, 2, 3, l \neq m$, we use $\mathcal{D}_1^{2h}(\mathcal{N}_{12}^{2h} \mathcal{D}_2^{2h})$ as an example and other cases are analogous,

$$\mathcal{D}_1^{2h} = \mathbf{I} \otimes D_1^{2h} \otimes \mathbf{I}_2 \otimes \mathbf{I}_3, \quad \mathcal{D}_2^{2h} = \mathbf{I} \otimes \mathbf{I}_1 \otimes D_2^{2h} \otimes \mathbf{I}_3,$$

where \mathbf{I} is a 3×3 identity matrix, \mathbf{I}_l , $l = 1, 2, 3$ are $n_l^{2h} \times n_l^{2h}$ identity matrices, D_1^{2h} is a $n_1^{2h} \times n_1^{2h}$ matrix defined in (5) for direction 1 and D_2^{2h} is a matrix of size $n_2^{2h} \times n_2^{2h}$ defined in (5) for direction 2. \mathcal{N}_{lm}^{2h} is a 3×3 block matrix with each block to be a $n_1^{2h}n_2^{2h}n_3^{2h} \times n_1^{2h}n_2^{2h}n_3^{2h}$ matrix

$$\mathcal{N}_{lm}^{2h} = \begin{pmatrix} N_{lm}^{11}(\mathbf{r}) & N_{lm}^{12}(\mathbf{r}) & N_{lm}^{13}(\mathbf{r}) \\ N_{lm}^{21}(\mathbf{r}) & N_{lm}^{22}(\mathbf{r}) & N_{lm}^{23}(\mathbf{r}) \\ N_{lm}^{31}(\mathbf{r}) & N_{lm}^{32}(\mathbf{r}) & N_{lm}^{33}(\mathbf{r}) \end{pmatrix}, \quad l = 1, 2, 3, m = 1, 2, 3, l \neq m. \quad (15)$$

Next, we approximate the elastic wave equation (1) on $\overline{\Gamma^f}$

$$\varrho_{\Gamma}^h(\mathbf{f}_{\Gamma})_{tt} = (\mathcal{J}_{\Gamma}^h)^{-1} \left(\sum_{l=1}^3 \left(\mathcal{G}_l^h(N_{ll})\mathbf{f} \Big|_{\Gamma} + \sum_{m=1, m \neq l}^3 \mathcal{D}_l^h(\mathcal{N}_{lm}^h \mathcal{D}_m^h \mathbf{f}) \Big|_{\Gamma} \right) \right) := L^h \mathbf{f} \Big|_{\Gamma}, \quad (16)$$

where ϱ_{Γ}^h and \mathcal{J}_{Γ}^h are $3n_1^h n_2^h (n_3^h - 1) \times 3n_1^h n_2^h (n_3^h - 1)$ diagonal matrix, which has a similar definition as in (13), but corresponds to the grids in $\overline{\Gamma^f}$. Lastly, we approximate the elastic wave equation (1) on Γ^f by

$$\varrho_{\Gamma}^h(\mathbf{f}_{\Gamma})_{tt} = (\mathcal{J}_{\Gamma}^h)^{-1} \left(\sum_{l=1}^3 \left(\mathcal{G}_l^h(N_{ll})\mathbf{f} \Big|_{\Gamma} + \sum_{m=1, m \neq l}^3 \mathcal{D}_l^h(\mathcal{N}_{lm}^h \mathcal{D}_m^h \mathbf{f}) \Big|_{\Gamma} \right) \right) + \boldsymbol{\eta} := L^h \mathbf{f} \Big|_{\Gamma} + \boldsymbol{\eta}, \quad (17)$$

with

$$\boldsymbol{\eta} = \varrho_{\Gamma}^h \tilde{\mathcal{P}} \left((\varrho^{2h})^{-1} \tilde{L}^{2h} \tilde{\mathbf{c}} \Big|_{\Gamma} \right) - L^h \mathbf{f} \Big|_{\Gamma}, \quad (18)$$

here, ϱ_{Γ}^h and \mathcal{J}_{Γ}^h are $3n_1^h n_2^h \times 3n_1^h n_2^h$ diagonal matrices with similar definitions as in (13) with grids on Γ^f . $(\varrho^{2h})^{-1} \tilde{L}^{2h} \tilde{\mathbf{c}} \Big|_{\Gamma}$ is a column vector of size $3n_1^h n_2^h$ and its value corresponds to the grids on Γ^c . In addition, the terms $\mathcal{G}_l^h(N_{ll})$, $l = 1, 2$ and $\mathcal{D}_l^h(\mathcal{N}_{lm}^h \mathcal{D}_m^h)$, $l = 1, 2, 3, m = 1, 2, 3, l \neq m$ in (16)–(17) have similar definitions as in (14)–(15), and $\mathcal{G}_3^h(N_{33})$ is defined by

$$\mathcal{G}_3^h(N_{33}) = \begin{pmatrix} G_3^h(N_{33}^{11}) & G_3^h(N_{33}^{12}) & G_3^h(N_{33}^{13}) \\ G_3^h(N_{33}^{21}) & G_3^h(N_{33}^{22}) & G_3^h(N_{33}^{23}) \\ G_3^h(N_{33}^{31}) & G_3^h(N_{33}^{32}) & G_3^h(N_{33}^{33}) \end{pmatrix},$$

where $G_3^h(N_{33}^{ij}(\mathbf{r}))$, $i, j = 1, 2, 3$, are $n_1^h n_2^h n_3^h \times n_1^h n_2^h n_3^h$ matrices which are defined as in (10) for direction 3. For the simplicity of analysis, we introduce a general notation for the schemes (16) and (17) in the fine domain Ω^f ,

$$\varrho^h \mathbf{f}_{tt} = \hat{L}^h \mathbf{f} = \begin{cases} L^h \mathbf{f} \Big|_{\Gamma} + \boldsymbol{\eta}, \\ L^h \mathbf{f} \Big|_{\overline{\Gamma}}. \end{cases} \quad (19)$$

In the following we are going to look at the interpolation operator \mathbf{P} and restriction operator \mathbf{R} in two dimensions. The stencils for the interpolation operator \mathbf{P} can be easily computed by a Taylor series expansion. In our case, we have the ratio of the mesh sizes for subdomain Ω^f and Ω^c is 1 : 2, then if \mathbf{P} is a fourth order interpolation operator in two dimensions, the stencils of \mathbf{P} are illustrated in Figure 3, the stencils for the corresponding restriction operator in two dimensions can be determined by the compatibility between interpolation and restriction operators, $\mathbf{P} = 4\mathbf{R}^T$, and its stencil is presented in Figure 4.

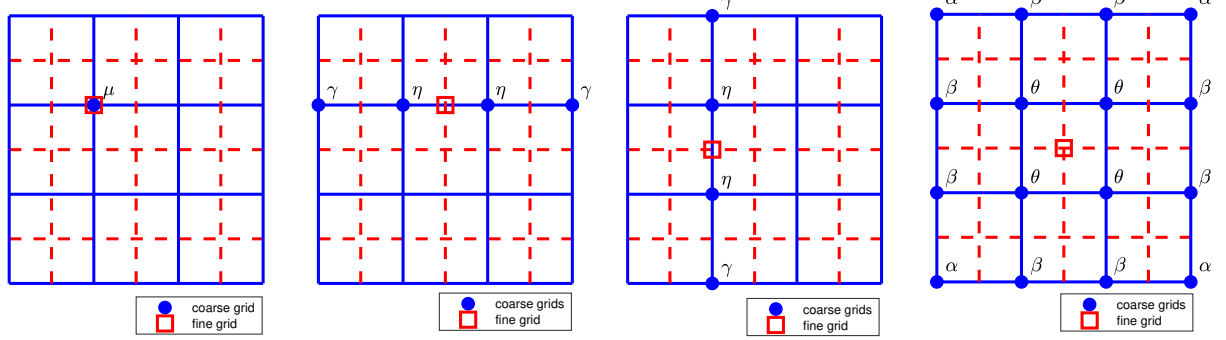


Figure 3: The sketch for the stencils of fourth order interpolation operator \mathbf{P} in two dimensions with parameters $\gamma = -\frac{1}{16}$, $\eta = \frac{9}{16}$, $\mu = 1$, $\alpha = \frac{1}{256}$, $\beta = -\frac{9}{256}$ and $\theta = \frac{81}{256}$.

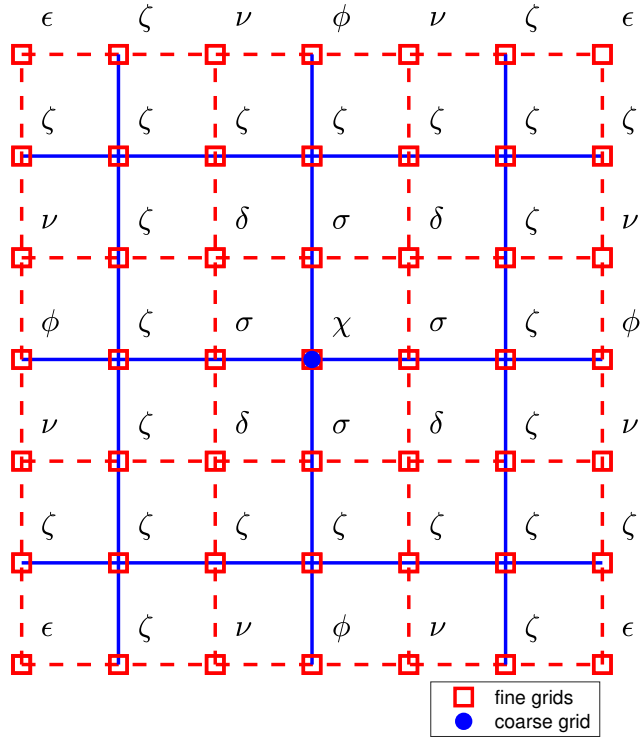


Figure 4: The sketch for the stencil of fourth order restriction operator \mathbf{R} in two dimensions with parameters $\epsilon = \frac{1}{1024}$, $\nu = -\frac{9}{1024}$, $\phi = -\frac{16}{1024}$, $\delta = \frac{81}{1024}$, $\sigma = \frac{144}{1024}$, $\chi = \frac{256}{1024}$ and $\zeta = 0$.

To proceed the interface conditions, we firstly introduce scaled interpolation and restriction operators

$$\tilde{\mathcal{P}} = (\mathcal{J}_\Gamma^h |\nabla_x^f r^3|)^{-\frac{1}{2}} \mathcal{P} (\mathcal{J}_\Gamma^{2h} |\nabla_x^c r^3|)^{\frac{1}{2}}, \quad \tilde{\mathcal{R}} = (\mathcal{J}_\Gamma^{2h} |\nabla_x^c r^3|)^{-\frac{1}{2}} \mathcal{R} (\mathcal{J}_\Gamma^h |\nabla_x^f r^3|)^{\frac{1}{2}}.$$

Here, \mathcal{P} is a $3n_1^{2h} n_2^{2h} n_3^{2h} \times 3n_1^{2h} n_2^{2h} n_3^{2h}$ matrix and \mathcal{R} is a $3n_1^h n_2^h n_3^h \times 3n_1^h n_2^h n_3^h$ matrix as

$$\mathcal{P} = \begin{pmatrix} \mathbf{P} & & \\ & \mathbf{P} & \\ & & \mathbf{P} \end{pmatrix}, \quad \mathcal{R} = \begin{pmatrix} \mathbf{R} & & \\ & \mathbf{R} & \\ & & \mathbf{R} \end{pmatrix}, \quad (20)$$

\mathbf{P} is a $n_1^{2h} n_2^{2h} n_3^{2h} \times n_1^{2h} n_2^{2h} n_3^{2h}$ matrix which has stencils as in Figure 3 and \mathbf{R} is a $n_1^h n_2^h n_3^h \times n_1^h n_2^h n_3^h$ matrix with a stencil as in Figure 4. Now, we are ready to state the continuous interface conditions (4), the grid functions \mathbf{f} and \mathbf{c} are coupled through interface conditions,

$$\mathbf{f}|_\Gamma = \tilde{\mathcal{P}}(\mathbf{c}|_\Gamma), \quad (21)$$

which imposes the continuity of the solution at the interface Γ and

$$|\nabla_x^c r^3|^{-1} (\mathcal{J}_\Gamma^{2h})^{-1} \tilde{\mathcal{A}}_3^{2h} \tilde{\mathbf{c}}|_\Gamma = \tilde{\mathcal{R}} \left(|\nabla_x^f r^3|^{-1} (\mathcal{J}_\Gamma^h)^{-1} (\mathcal{A}_3^h \mathbf{f}|_\Gamma - h\omega_1 \mathcal{J}^h \boldsymbol{\eta}) \right) \quad (22)$$

where we have used the notations

$$\mathcal{A}_3^h \mathbf{f}|_\Gamma = \mathcal{N}_{31}^h \mathcal{D}_1^h \mathbf{f}|_\Gamma + \mathcal{N}_{32}^h \mathcal{D}_2^h \mathbf{f}|_\Gamma + \mathcal{N}_{33}^h \mathcal{D}_3^h \mathbf{f}|_\Gamma, \quad (23)$$

and

$$\tilde{\mathcal{A}}_3^{2h} \tilde{\mathbf{c}}|_\Gamma = \mathcal{N}_{31}^{2h} \mathcal{D}_1^{2h} \mathbf{c}|_\Gamma + \mathcal{N}_{32}^{2h} \mathcal{D}_2^{2h} \mathbf{c}|_\Gamma + \mathcal{N}_{33}^{2h} \tilde{\mathcal{D}}_3^{2h} \tilde{\mathbf{c}}|_\Gamma, \quad (24)$$

which imposes the continuity of traction at the interface Γ , here, ω_1 is the first entry in the scalar product (6), and $\tilde{\mathcal{D}}_3^{2h}$ is defined as

$$\tilde{\mathcal{D}}_3^{2h} = \mathbf{I} \otimes \mathbf{I}_1 \otimes \mathbf{I}_2 \otimes \tilde{D}_3^{2h}$$

where \mathbf{I} is a 3×3 identity matrix, $\mathbf{I}_l, l = 1, 2$ are $n_l^{2h} \times n_l^{2h}$ identity matrices, \tilde{D}_3^{2h} is a $n_3^{2h} \times (n_3^{2h} + 2)$ matrix defined in (7) for direction 3.

3.3 Energy estimate

In this section, we investigate the energy estimate for the semi-discrete forms (12) and (19) in section 3.2. Provided periodic boundary conditions in directions 1 and 2. Let \mathbf{u}, \mathbf{v} be grid functions in Ω^c . We define the three dimensional scalar product in Ω^c

$$(\mathbf{u}, \mathbf{v})_{2h} = 8h_1 h_2 h_3 \sum_{i=1}^{n_1^{2h}} \sum_{j=1}^{n_2^{2h}} \sum_{k=1}^{n_3^{2h}} \omega_k J_{ijk}^{2h} u_{ijk} v_{ijk}, \quad (25)$$

where J_{ijk}^{2h} located at the $((k-1)n_1^{2h} n_2^{2h} + (j-1)n_1^{2h} + i)$ 'th row and $((k-1)n_1^{2h} n_2^{2h} + (j-1)n_1^{2h} + i)$ 'th column of \mathbf{J}^{2h} , u_{ijk} and v_{ijk} located at the $((k-1)n_1^{2h} n_2^{2h} + (j-1)n_1^{2h} + i)$ 'th row of \mathbf{u}, \mathbf{v} respectively. The two dimensional scalar product for grid functions on the interface Γ^c

$$\langle \mathbf{u}_{\Gamma^c}, \mathbf{v}_{\Gamma^c} \rangle_{2h} = 4h_1 h_2 \sum_{i=1}^{n_1^{2h}} \sum_{j=1}^{n_2^{2h}} J_{\Gamma,ij}^{2h} |\nabla_x^c r^3|_{ij} u_{ij} v_{ij}. \quad (26)$$

with $J_{\Gamma,ij}^{2h}$ located at the $((j-1)n_1^{2h} + i)$ 'th row and $((j-1)n_1^{2h} + i)$ 'th column of diagonal matrix \mathbf{J}_{Γ}^{2h} , u_{ij} , v_{ij} are the $((j-1)n_1^{2h} + i)$ 'th element of u_{Γ^c} and v_{Γ^f} respectively. On the other hand, let \mathbf{u}, \mathbf{v} be grid functions in Ω^f . We define the three dimensional discrete scalar product in Ω^f similarly as in Ω^c

$$(\mathbf{u}, \mathbf{v})_h = h_1 h_2 h_3 \sum_{i=1}^{n_1^h} \sum_{j=1}^{n_2^h} \sum_{k=1}^{n_3^h} \omega_k J_{ijk}^h u_{ijk} v_{ijk},$$

and the two dimensional scalar product for grid functions on the interface Γ^f

$$\langle \mathbf{u}_{\Gamma^f}, \mathbf{v}_{\Gamma^f} \rangle_h = h_1 h_2 \sum_{i=1}^{n_1^h} \sum_{j=1}^{n_2^h} J_{\Gamma,ij}^h |\nabla_x^f r^3|_{ij} u_{ij} v_{ij}, \quad (27)$$

where J_{ijk}^h , u_{ijk} , v_{ijk} , $J_{\Gamma,ij}^h$, u_{ij} and v_{ij} have similar definitions as in (25) and (26).

Now, we are ready to present the energy conservation of the proposed schemes in Section 3.2. Multiplying (12) by $8h_1 h_2 h_3 \omega_k \mathcal{J}^{2h} \mathbf{c}_t$ and summing over all grids, we have

$$(\mathbf{c}_t, \varrho^{2h} \mathbf{c}_{tt})_{2h} = (\mathbf{c}_t, \tilde{L}^{2h} \tilde{\mathbf{c}})_{2h} = -S_{2h}(\mathbf{c}_t, \mathbf{c}) + B_{2h}(\mathbf{c}_t, \tilde{\mathbf{c}}), \quad (28)$$

multiplying (19) by $h_1 h_2 h_3 \omega_k \mathcal{J}^h \mathbf{f}_t$ and summing over all grids, we obtain

$$(\mathbf{f}_t, \varrho^h \mathbf{f}_{tt})_h = (\mathbf{f}_t, \hat{L}^h \mathbf{f})_h = -S_h(\mathbf{f}_t, \mathbf{f}) + B_h(\mathbf{f}_t, \mathbf{f}) + h_1 h_2 h_3 \omega_1 (\mathbf{f}_\Gamma)_t^T \boldsymbol{\eta},$$

where both S_{2h} and S_h are symmetric and positive definite bilinear forms, and

$$B_h(\mathbf{f}_t, \mathbf{f}) = -h_1 h_2 (\mathbf{f}_\Gamma)_t^T (\mathcal{N}_{31}^h \mathcal{D}_1^h \mathbf{f}|_\Gamma + \mathcal{N}_{32}^h \mathcal{D}_2^h \mathbf{f}|_\Gamma + \mathcal{N}_{33}^h \mathcal{D}_3^h \mathbf{f}|_\Gamma), \quad (29)$$

and

$$B_{2h}(\mathbf{c}_t, \tilde{\mathbf{c}}) = 4h_1 h_2 (\mathbf{c}_\Gamma)_t^T (\mathcal{N}_{31}^{2h} \mathcal{D}_1^{2h} \mathbf{c}|_\Gamma + \mathcal{N}_{32}^{2h} \mathcal{D}_2^{2h} \mathbf{c}|_\Gamma + \mathcal{N}_{33}^{2h} \tilde{\mathcal{D}}_3^{2h} \tilde{\mathbf{c}}|_\Gamma). \quad (30)$$

Then, the time derivative of the semi-discrete energy reads as

$$\begin{aligned} \frac{d}{dt} [(\mathbf{f}_t, \varrho^h \mathbf{f}_t)_h + S_h(\mathbf{f}, \mathbf{f}_t) + (\mathbf{c}_t, \varrho^{2h} \mathbf{c}_t)_{2h} + S_{2h}(\mathbf{c}, \mathbf{c}_t)] = \\ 2B_h(\mathbf{f}_t, \mathbf{f}) + 2B_{2h}(\mathbf{c}_t, \tilde{\mathbf{c}}) + 2h_1 h_2 h_3 \omega_1 (\mathbf{f}_\Gamma)_t^T \boldsymbol{\eta}, \end{aligned} \quad (31)$$

plugging (29)–(30) into (31) and combining the definition of the scalar product on the interface Γ (26)–(27), we have

$$\begin{aligned} & \frac{d}{dt} \left[(\mathbf{f}_t, \varrho^h \mathbf{f}_t)_h + S_h(\mathbf{f}, \mathbf{f}_t) + (\mathbf{c}_t, \varrho^{2h} \mathbf{c}_t)_{2h} + S_{2h}(\mathbf{c}, \mathbf{c}_t) \right] \\ &= 2 \left\langle (\mathbf{f}_\Gamma)_t, |\nabla^f r^3|^{-1} (\mathcal{J}_\Gamma^h)^{-1} (-\mathcal{A}_3^h \mathbf{f}|_\Gamma + h\omega_1 \boldsymbol{\eta}) \right\rangle_h + 2 \left\langle (\mathbf{c}_\Gamma)_t, |\nabla^c r^3|^{-1} (\mathcal{J}_\Gamma^{2h})^{-1} \tilde{\mathcal{A}}_3^{2h} \tilde{\mathbf{c}}|_\Gamma \right\rangle_{2h} \\ &= 2 \left\langle (\mathbf{f}_\Gamma)_t, |\nabla^f r^3|^{-1} (\mathcal{J}_\Gamma^h)^{-1} (-\mathcal{A}_3^h \mathbf{f}|_\Gamma + h\omega_1 \boldsymbol{\eta}) \right\rangle_h + 2 \left\langle (\mathbf{c}_\Gamma)_t, |\nabla^c r^3|^{-1} (\mathcal{J}_\Gamma^{2h})^{-1} \tilde{\mathcal{A}}_3^{2h} \tilde{\mathbf{c}}|_\Gamma \right\rangle_{2h} \\ &= 2 \left\langle (\mathbf{c}_\Gamma)_t, \tilde{\mathcal{R}}(|\nabla^f r^3|^{-1} (\mathcal{J}_\Gamma^h)^{-1} (-\mathcal{A}_3^h \mathbf{f}|_\Gamma + h\omega_1 \boldsymbol{\eta})) \right\rangle_{2h} + 2 \left\langle (\mathbf{c}_\Gamma)_t, |\nabla^c r^3|^{-1} (\mathcal{J}_\Gamma^{2h})^{-1} \tilde{\mathcal{A}}_3^{2h} \tilde{\mathbf{c}}|_\Gamma \right\rangle_{2h} = 0, \end{aligned}$$

where we have used the notaions in (23)–(24).

4 The temporal discretization

The equations are advanced in time with an explicit fourth order accurate predictor-corrector time integration method. Like all explicit time stepping methods, there is a maximum time step not exceed CFL stability limit.

In [5], it is proved that the time step constraint by CFL condition for the Newmark scheme

$$\varrho^h \frac{\mathbf{f}^{n+1} - 2\mathbf{f}^n + \mathbf{f}^{n-1}}{\Delta_t^2} = \hat{L}^h \mathbf{f}^n, \quad \varrho^{2h} \frac{\mathbf{c}^{n+1} - 2\mathbf{c}^n + \mathbf{c}^{n-1}}{\Delta_t^2} = \tilde{L}^{2h} \tilde{\mathbf{c}}^n, \quad n = 0, 1, \dots,$$

which is second order with

$$\frac{\Delta_t^2}{h^2} \kappa_{\max} \leq C_{\text{cfl}}^2$$

for the elastic wave equation with a homogeneous material and periodic boundary conditions, provided $h_1 = h_2 = h_3 = h$. Here, κ_{\max} is the maximum of the eigenvalue of the matrices

$$T_{\mathbf{i}}^{\{f,c\}} = \frac{1}{\rho^{\{f,c\}}(\mathbf{r}_i)} \begin{pmatrix} Tr(N_{11}^{\{f,c\}}(\mathbf{r}_i)) & Tr(N_{12}^{\{f,c\}}(\mathbf{r}_i)) & Tr(N_{13}^{\{f,c\}}(\mathbf{r}_i)) \\ Tr(N_{21}^{\{f,c\}}(\mathbf{r}_i)) & Tr(N_{22}^{\{f,c\}}(\mathbf{r}_i)) & Tr(N_{23}^{\{f,c\}}(\mathbf{r}_i)) \\ Tr(N_{31}^{\{f,c\}}(\mathbf{r}_i)) & Tr(N_{32}^{\{f,c\}}(\mathbf{r}_i)) & Tr(N_{33}^{\{f,c\}}(\mathbf{r}_i)) \end{pmatrix},$$

where $Tr(N_{ij}^{\{f,c\}}(\mathbf{r}_i))$ represents the trace of 3×3 matrix $N_{ij}^{\{f,c\}}(\mathbf{r}_i)$, $i, j = 1, 2, 3$. In this paper, we use the predictor-corrector strategy to obtain a fourth order time integrator. In [6], it shows that the fourth order scheme has a somewhat larger stability limit for the time step, but the way used to approximate eigenvalue is same. We use $C_{\text{cfl}} = 1.3175$ in the numerical experiments in this paper.

4.1 Time discretization with SBP scheme

In the following, we give the detailed procedures about how we apply the fourth order time integrator to the problems (12) and (19).

Let \mathbf{c}^n and \mathbf{f}^n denote the numerical approximations of $\mathbf{C}(\mathbf{x}, t_n)$, $\mathbf{x} \in \Omega^c$ and $\mathbf{F}(\mathbf{x}, t_n)$, $\mathbf{x} \in \Omega^f$ respectively. Here, $t_n = n\Delta_t$, $n = 0, 1, \dots$ and $\Delta_t > 0$ is a constant time step. We present the fourth order time integrator with predictor and corrector in the Algorithm 1.

Algorithm 1 Fourth order accurate time stepping for the elastic wave equation with SBP discretization in space

Given initial conditions $\tilde{\mathbf{c}}^0, \tilde{\mathbf{c}}^{-1}$ and $\mathbf{f}^0, \mathbf{f}^{-1}$ that satisfies the discretized interface conditions.

- Compute the predictor at the interior grid points for both fine and coarse domains

$$\mathbf{c}^{*,n+1} = 2\mathbf{c}^n - \mathbf{c}^{n-1} + \Delta_t^2 (\varrho^{2h})^{-1} \tilde{L}^{2h} \tilde{\mathbf{c}}^n, \quad \mathbf{f}^{*,n+1} = 2\mathbf{f}^n - \mathbf{f}^{n-1} + \Delta_t^2 (\varrho^h)^{-1} \hat{L}^h \mathbf{f}^n$$

- For the continuity of solution on the interface Γ , assign the value $\mathbf{f}_{\Gamma}^{*,n+1}$ to satisfy

$$\mathbf{f}_{\Gamma}^{*,n+1} = \tilde{\mathcal{P}}(\mathbf{c}_{\Gamma}^{*,n+1})$$

- For the continuity of traction on the interface Γ , assign the ghost points value in $\tilde{\mathbf{c}}^{*,n+1}$ to satisfy

$$|\nabla_x^c r^3|^{-1} (\mathcal{J}_{\Gamma}^{2h})^{-1} \tilde{\mathcal{A}}_3^{2h} \tilde{\mathbf{c}}^{*,n+1}|_{\Gamma} = \tilde{\mathcal{R}} \left(|\nabla_x^f r^3|^{-1} (\mathcal{J}_{\Gamma}^h)^{-1} (\mathcal{A}_3^h \mathbf{f}^{*,n+1}|_{\Gamma} - h_3 \omega_1 \boldsymbol{\eta}^{*,n+1}) \right) \quad (32)$$

with the definition of $\tilde{\mathcal{A}}_3^{2h}$ in (24), \mathcal{A}_3^h in (23)

- Evaluate the acceleration at all grids

$$\tilde{\mathbf{c}}^n = \frac{\tilde{\mathbf{c}}^{*,n+1} - 2\tilde{\mathbf{c}}^n + \tilde{\mathbf{c}}^{n-1}}{\Delta_t^2}, \quad \mathbf{f}^n = \frac{\mathbf{f}^{*,n+1} - 2\mathbf{f}^n + \mathbf{f}^{n-1}}{\Delta_t^2}$$

- Compute the corrector at the interior grid points

$$\mathbf{c}^{n+1} = \mathbf{c}^{*,n+1} + \frac{\Delta_t^4}{12}(\varrho^{2h})^{-1}\tilde{L}^{2h}\tilde{\mathbf{c}}^n, \quad \mathbf{f}^{n+1} = \mathbf{f}^{*,n+1} + \frac{\Delta_t^4}{12}(\varrho^h)^{-1}\hat{L}^h\mathbf{f}^n$$

- For the continuity of solution on the interface Γ , assign the value \mathbf{f}_Γ^{n+1} to satisfy

$$\mathbf{f}_\Gamma^{n+1} = \tilde{\mathcal{P}}(\mathbf{c}_\Gamma^{n+1})$$

- For the continuity of traction on the interface Γ , assign the ghost point value in $\tilde{\mathbf{c}}^{n+1}$ to satisfy

$$|\nabla_x^c r^3|^{-1} (\mathcal{J}_\Gamma^{2h})^{-1} \tilde{\mathcal{A}}_3^{2h} \tilde{\mathbf{c}}^{n+1} \Big|_\Gamma = \tilde{\mathcal{R}} \left(|\nabla_x^f r^3|^{-1} (\mathcal{J}_\Gamma^h)^{-1} (\mathcal{A}_3^h \mathbf{f}^{n+1}) \Big|_\Gamma - h_3 \omega_1 \boldsymbol{\eta}^{n+1} \right) \quad (33)$$

with the definition of $\tilde{\mathcal{A}}_3^{2h}$ in (24), \mathcal{A}_3^h in (23)

Here, we only give the steps to evolve the elatic wave equation with suitable initial and interface conditions and skip the detailed derivations of the fourth order predictor corrector time integrator. One can refer [8] to get more details.

In the Algorithm 1, we need to solve the equations come from the continuity of the traction force for the interface Γ in both preditor step (32) and corrector step (33). The structure of (32) and (33) are same, for simplicity, we only clarify how we solve (32) in the predictor step.

Note that there are $3n_1^{2h}n_2^{2h}$ unknowns in (32) and $3n_1^{2h}n_2^{2h}$ linear equations in (32). Since it is very expensive to calculate the LU-factorization for a large problem in 3D and there is no efficient ways to calculate the LU-factorization in a parallel machine, we instead using iterative methods to solve the linear system (32). Specifically, we use three different iterative methods: block Jacobian iterative method, conjugate gradient iterative method and pre-conditioned conjugate gradient iterative method to solve (32). The details are given in Section 5.1.1.

5 Numerical Experiments

In this section, we conduct several numerical experiments. In Section 5.1, we compare the efficiency of iterative methods which are used to solve the interface condition system (32) and (33), note that the coefficient matrices in (32) and (33) are same; verify the order of the convergence of the proposed scheme (12), (19) and (21)–(22). In Section 5.2, we show that there is no obvious reflection at the mesh refinement interface for the proposed scheme (12), (19) and (21)–(22) with only a traction force on the top surface. Finally, the energy conservation property is shown in Section 5.3.

5.1 Method of manufactured solutions

We take the computation domain to be

$$\begin{cases} x^{c,1} = 2\pi r^1 \\ x^{c,2} = 2\pi r^2 \\ x^{c,3} = r^3 \theta_i(r^1, r^2) + (1 - r^3) \theta_b(r^1, r^2) \end{cases} \quad (34)$$

for coarse domain Ω^c . Here, $0 \leq r^1, r^2, r^3 \leq 1$, f_i is the interface surface geometry,

$$\theta_i(r^1, r^2) = \pi + 0.2 \sin(4\pi r^1) + 0.2 \cos(4\pi r^2), \quad (35)$$

and θ_b is the bottom surface geometry,

$$\theta_b(r^1, r^2) = 0.2 \exp\left(-\frac{(r^1 - 0.6)^2}{0.04}\right) + 0.2 \exp\left(-\frac{(r^2 - 0.6)^2}{0.04}\right). \quad (36)$$

As for the fine domain Ω^f , it is chosen to be

$$\begin{cases} x^{f,1} = 2\pi r^1 \\ x^{f,2} = 2\pi r^2 \\ x^{f,3} = r^3 \theta_t(r^1, r^2) + (1 - r^3) \theta_i(r^1, r^2), \end{cases} \quad (37)$$

where $0 \leq r^1, r^2, r^3 \leq 1$, θ_t is the top surface geometry,

$$\theta_t(r^1, r^2) = 0.2 \exp\left(-\frac{(r^1 - 0.5)^2}{0.04}\right) + 0.2 \exp\left(-\frac{(r^2 - 0.5)^2}{0.04}\right), \quad (38)$$

and θ_i is the interface geometry which is given in (35). Note that the subdomain Ω^f is on the top of the subdomain Ω^c . For both fine and coarse domains, let the density vary according to

$$\rho(x^1, x^2, x^3) = 2 + \sin(x^1 + 0.3) \sin(x^2 + 0.3) \sin(x^3 - 0.2), \quad (39)$$

and material parameters μ, λ satisfy

$$\mu(x^1, x^2, x^3) = 3 + \sin(3x^1 + 0.1) \sin(3x^2 + 0.1) \sin(x^3), \quad (40)$$

and

$$\lambda(x^1, x^2, x^3) = 21 + \cos(x^1 + 0.1) \cos(x^2 + 0.1) \sin^2(3x^3), \quad (41)$$

respectively. Besides, we impose a boundary forcing on the top surface and Dirichlet boundary conditions for the other boundaries. The external forcing, top boundary forcing \mathbf{g} and initial conditions are chosen such that $\mathbf{u}(\cdot, t) = (u_1(\cdot, t), u_2(\cdot, t), u_3(\cdot, t))^T$ with

$$\begin{aligned} u_1(\cdot, t) &= \cos(x^1 + 0.3) \sin(x^2 + 0.3) \sin(x^3 + 0.2) \cos(t^2), \\ u_2(\cdot, t) &= \sin(x^1 + 0.3) \cos(x^2 + 0.3) \sin(x^3 + 0.2) \cos(t^2), \\ u_3(\cdot, t) &= \sin(x^1 + 0.2) \sin(x^2 + 0.2) \cos(x^3 + 0.2) \sin(t). \end{aligned}$$

For example, for the boundary forcing on the top surface, we impose

$$\mathbf{g} = (g_1, g_2, g_3)^T = \sum_{i=1}^3 \left(\sum_{j=1}^3 M_{ij}^f \frac{\partial \mathbf{u}}{\partial x^{(j)}} \right) n_3^{f,+i}, \quad (42)$$

where, M_{ij}^f and $n_3^{f,+i}$ can be found in (2) and (3) respectively.

5.1.1 Iterative methods

In the proposed scheme (12), (19) and (21)–(22), we need to solve a $3n_1^{2h}n_1^{2h} \times 3n_1^{2h}n_1^{2h}$ linear system at each time step twice for the continuity of the traction force along the interface (32) and (33). Even though we can LU factorize the linear system before the time loop and reuse it at each time step, it is very expensive and memory inefficient to do LU factorization for a large problem in 3D. Besides, consider solving real problems which are usually in large scale, we want to perform the computation on many processors on a parallel distributed memory machine, but it is not clear how to calculate the LU factorization of a matrix on many processors.

We have considered three iterative methods: the block Jacobian method, the conjugate gradient method, and the preconditioned conjugate gradient method. We note that the linear system arising from the interface conditions is indefinite. However, our experiment show that both the conjugate gradient method and the preconditioned conjugate gradient method converge. Except the following test that compares the three iterative methods, we always use the block Jacobian method to guarantee that the whole scheme converges.

For the problem proposed in Section 5.1, the structure of the coefficient matrix of the linear system (22) is shown in Figure 5 which is determined by the interpolation operator $\tilde{\mathcal{P}}$ and restriction operator $\tilde{\mathcal{R}}$. We choose the red circles in the purple circles in Figure 5 to be the block Jacobian matrix in block Jacobian iterative method and pre-conditioning matrix in pre-conditioned conjugate gradient iterative method. The absolute error tolerance is set to be $1e-7$ for each iterative method and $h_1 = h_2 = h_3 = h$.

$2h$	CG	Block Jacobian	Preconditioned CG
$2\pi/24$	37.78	24.96	4.01
$2\pi/48$	38.61	25.38	2.87
$2\pi/96$	39.14	25.43	2.25

Table 1: condition number of matrices in conjugate gradient method, block Jacobian method, preconditioned conjugate gradient method

Table 1 shows the condition number of the original coefficient matrix, the block Jacobian matrix and the coefficient matrix after applying pre-conditioner respectively. We observe that the condition number for preconditioned conjugate gradient method is smallest which is consistent with the results of iteration number for different iterative methods : there is around 44 iterations for conjugate gradient method, 13 iterations for block Jacobian method and 9 iterations for preconditioned conjugate method.

In comparison, we have also performed an LU factorization for the linear system when the mesh size $2h = 2\pi/96$, and the computation takes 40.6 GB memory. In contrast, with the block Jacobian method, the peak memory usage is only 1.2 GB. For large-scale problems, the memory usage becomes infeasible for the LU factorization.

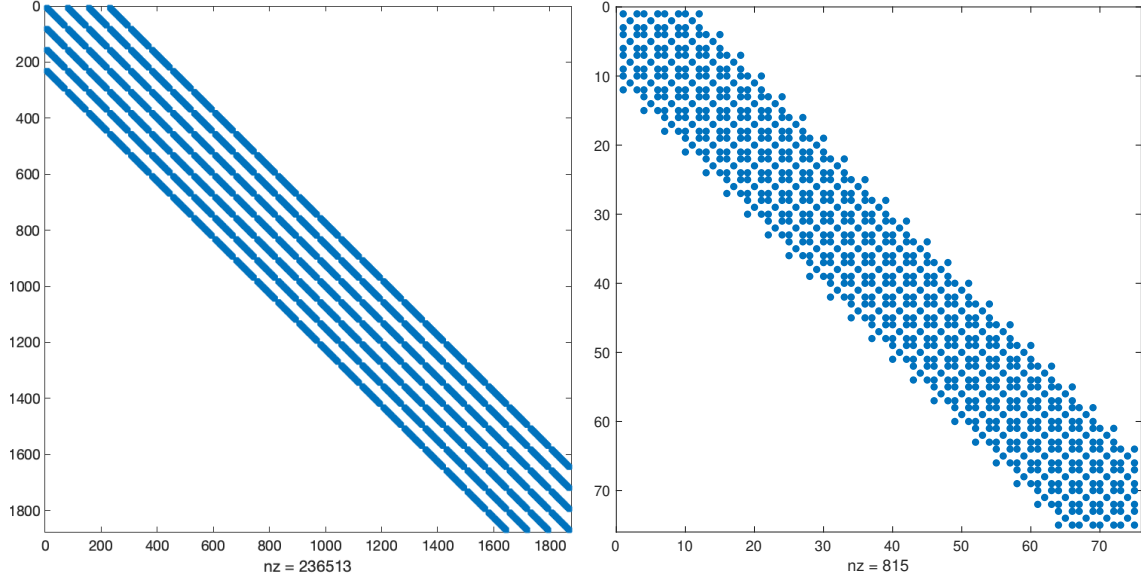


Figure 5: The left panel is the structure of the coefficient matrix of the linear system (22). The right panel is the zoom in structure for the repeated pattern on the left panel.

5.1.2 Verification of convergence rate

We now perform a convergence study for the proposed scheme (12), (19) and (21)–(22). The convergence rate is computed by

$$\log\left(\frac{e_h}{e_{2h}}\right) \Big/ \log\left(\frac{1}{2}\right),$$

here, e_h is the corresponding L^2 error. The problem is evolved until final time $T = 0.5$. The L^2 error for the numerical solutions in the whole domain, $L^{f,2}$ error for the numerical solutions in the fine domain Ω^f and $L^{c,2}$ error for the numerical solutions in the coarse domain Ω^c are presented in Table 2. We observe that the convergence rate is fourth order for all cases, though the theoretical convergence rate is second for the points near boundaries. Note that we use a block Jacobian iterative method for the experiments here.

$2h_1 = 2h_2 = 2h_3 = 2h$	L^2	$L^{f,2}$	$L^{c,2}$
$2\pi/24$	2.2227e-03	8.0442e-04	2.0720e-03
$2\pi/48$	1.4142e-04 (3.97)	5.1478e-05 (3.97)	1.3171e-04 (3.98)
$2\pi/96$	8.6166e-06 (4.04)	3.0380e-06 (4.08)	8.0632e-06 (4.03)

Table 2: Convergence rate of the fourth order SBP method

5.2 Gaussian source

In this section, we present the numerical experiments to illustrate that there is no obvious artifacts are generated by the curvilinear interface. Specifically, we test the problem on the computation

domain

$$\begin{cases} x^{c,1} = 2000r^1 \\ x^{c,2} = 2000r^2 \\ x^{c,3} = r^3\theta_i(r^1, r^2) + (1 - r^3)\theta_b(r^1, r^2) \end{cases} \quad (43)$$

for coarse domain Ω^c . Here, $0 \leq r^1, r^2, r^3 \leq 1$, θ_i is the interface surface geometry,

$$\theta_i(r^1, r^2) = 800 + 20 \sin(4\pi r^1) + 20 \cos(4\pi r^2), \quad (44)$$

and θ_b is the bottom surface geometry,

$$\theta_b(r^1, r^2) = 0. \quad (45)$$

As for the fine domian Ω^f , it is choose to be

$$\begin{cases} x^{f,(1)} = 2000r^1 \\ x^{f,(2)} = 2000r^2 \\ x^{f,(3)} = r^3\theta_t(r^1, r^2) + (1 - r^3)\theta_i(r^1, r^2), \end{cases} \quad (46)$$

where $0 \leq r^1, r^2, r^3 \leq 1$, θ_t is the top surface geometry,

$$\theta_t(r^1, r^2) = 1000, \quad (47)$$

and θ_i is the interface geometry which is given in (44). Note that the subdomian Ω^f is on the top of subdomain Ω^c . For both fine and coarse domians, let the density vary according to

$$\rho(x^1, x^2, x^3) = 1.5 \times 10^3, \quad (48)$$

and material parameters μ, λ satisfy

$$\mu(x^1, x^2, x^3) = 1.5 \times 10^9, \quad \lambda(x^1, x^2, x^3) = 3 \times 10^9, \quad (49)$$

respectively. Besides, we impose a Gaussian source on the top surface

$$\mathbf{g} = (g_1, g_2, g_3)^T,$$

where, $g_1 = g_2 = 0$, and

$$g_3 = 10^9 \exp \left(- \left(\frac{t - 4/44.2}{1/44.2} \right)^2 \right) \exp \left(- \left(\frac{x^1 - 1000}{12.5} \right)^2 - \left(\frac{x^2 - 1000}{12.5} \right)^2 \right).$$

Homogeneous Dirichlet boundary conditions are imposed to the other boundaries. The external forcing is choosen to be zeros everywhere and the initial condition is also setted to be zero everywhere, $\mathbf{u} = \mathbf{0}$ at $t = 0$.

To compare the results, we use the solutions from a flat interface surface, $\theta_i(r^1, r^2) = 0$, with only Cartesian grids and no mesh refinement. Specifically, denote $(n_1^{2h}, n_2^{2h}, n_3^{2h})$ to be the number of grid points in the coarse domian Ω^c , (n_1^h, n_2^h, n_3^h) to be the number of grid points in the fine domian Ω^f , (n_1, n_2, n_3) to be the number of grid points for the reference solution.

In the simulation of the reference solution, we choose $n_1 = n_2 = 201, n_3 = 101$. And in the experiments for the curvilinear interface with mesh refinement, we have $n_1^{2h} = n_2^{2h} = 101, n_3^{2h} = 41$ and $n_1^h = n_2^h = 201, n_3^h = 21$. The numerical simulations are conducted until $T = 0.4$.

From Figure 6, Figure 7 and Figure 8, we observe that there is no significant reflection at the mesh refinement interface.

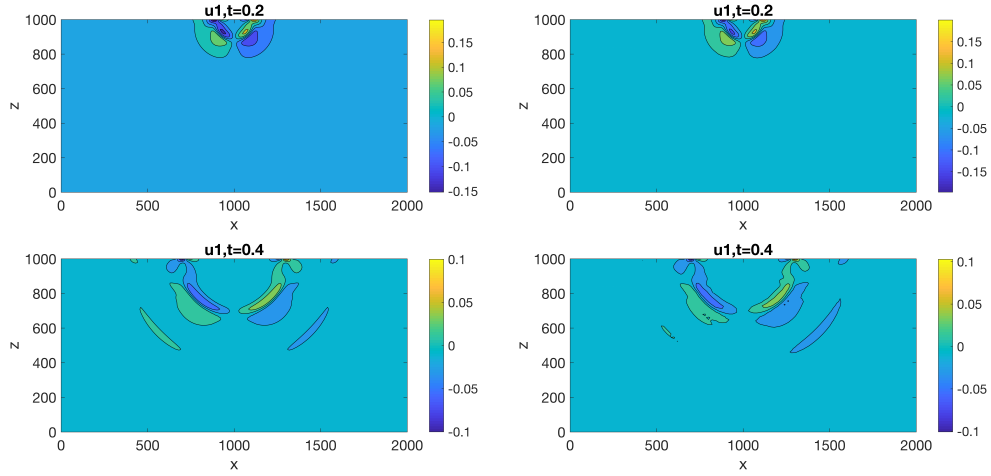


Figure 6: The graph for u_1 . From left to right are for Cartesian mesh without mesh refinement interface and curvi-linear mesh with mesh refinement interface respectively. From top to bottom are for $t = 0.2$ and $t = 0.4$ respectively.

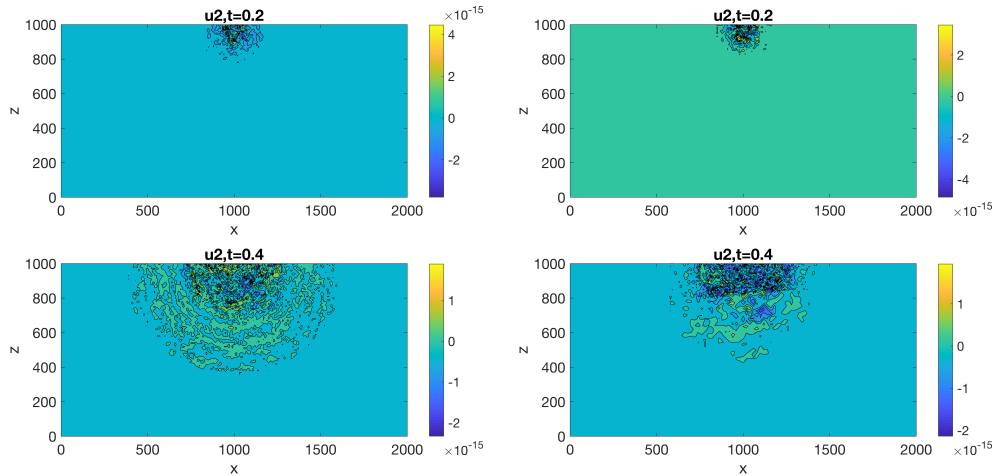


Figure 7: The graph for u_2 . From left to right are for Cartesian mesh without mesh refinement interface and curvi-linear mesh with mesh refinement interface respectively. From top to bottom are for $t = 0.2$ and $t = 0.4$ respectively.

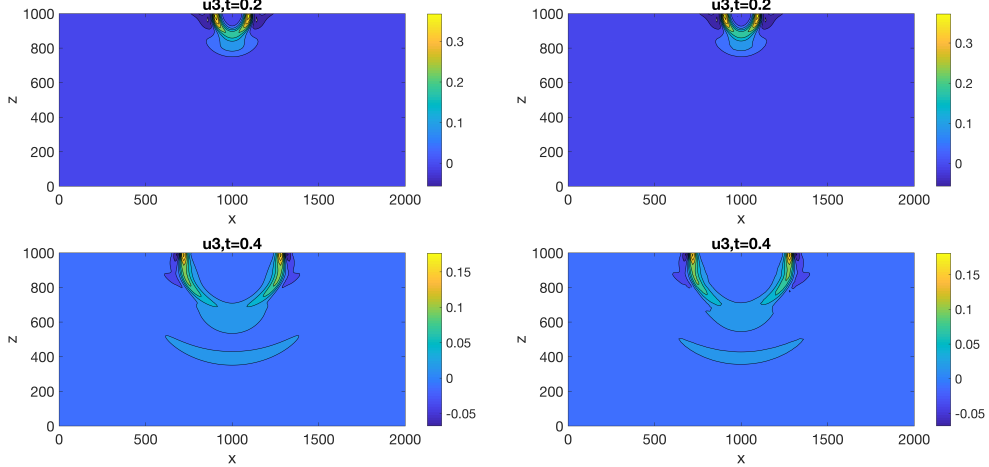


Figure 8: The graph for u_3 . From left to right are for Cartesian mesh without mesh refinement interface and curvi-linear mesh with mesh refinement interface respectively. From top to bottom are for $t = 0.2$ and $t = 0.4$ respectively.

5.3 Energy conservation test

To verify the energy conservation property of our scheme, we perform a computation without external source term, but with a Gaussian initial profile which centered at the origin of the computational domain. Specifically, the computational domain, density function ρ and material functions μ, λ are taken to be the same as in the Section 5.1; the initial Gaussian profiles are

$$\begin{aligned} u_1(\cdot, 0) &= \exp\left(-\frac{(x^1 - \pi)^2}{0.1}\right) \exp\left(-\frac{(x^2 - \pi)^2}{0.1}\right) \exp\left(-\frac{(x^3 - \pi)^2}{0.1}\right), \\ u_2(\cdot, 0) &= \exp\left(-\frac{(x^1 - \pi)^2}{0.2}\right) \exp\left(-\frac{(x^2 - \pi)^2}{0.2}\right) \exp\left(-\frac{(x^3 - \pi)^2}{0.2}\right), \\ u_3(\cdot, 0) &= \exp\left(-\frac{(x^1 - \pi)^2}{0.1}\right) \exp\left(-\frac{(x^2 - \pi)^2}{0.2}\right) \exp\left(-\frac{(x^3 - \pi)^2}{0.2}\right). \end{aligned}$$

Energy conservation is ensured by homogeneous Dirichlet boundary conditions. The grid spacing is $h_1 = h_2 = h_3 = h$ and $2h = \frac{\pi}{12}$ for coarse domain Ω^c , $h = \frac{\pi}{24}$ for fine domain Ω^f , thus we have $25 \times 25 \times 13$ grid points in the coarse domain Ω^c and $49 \times 49 \times 25$ grid points in the fine domain Ω^f .

For the semi-discrete approximation, the energy is given by $(\mathbf{f}_t, \varrho^h \mathbf{f}_t)_h + S_h(\mathbf{f}, \mathbf{f}_t) + (\mathbf{c}_t, \varrho^{2h} \mathbf{c}_t)_{2h} + S_{2h}(\mathbf{c}, \mathbf{c}_t)$, see (31). By using a same approach as for the isotropic elastic wave equation, see [5, 6], the expression for the fully discrete energy reads as

$$\begin{aligned} E^{n+1/2} &= \left\| \sqrt{\varrho^h} \frac{\mathbf{f}^{n+1} - \mathbf{f}^n}{\Delta t} \right\|_h^2 + S_h(\mathbf{f}^{n+1}, \mathbf{f}^n) - \frac{(\Delta t)^2}{12} (L^h \mathbf{f}^{n+1}, L^h \mathbf{f}^n)_h \\ &\quad + \left\| \sqrt{\varrho^{2h}} \frac{\mathbf{c}^{n+1} - \mathbf{c}^n}{\Delta t} \right\|_{2h}^2 + S_{2h}(\mathbf{c}^{n+1}, \mathbf{c}^n) - \frac{(\Delta t)^2}{12} (\tilde{L}^{2h} \tilde{\mathbf{c}}^{n+1}, \tilde{L}^{2h} \tilde{\mathbf{c}}^n)_{2h}. \end{aligned}$$

We present the relative change in fully discrete energy, $(E^{n+1/2} - E^{1/2})/E^{1/2}$, as a function of time with $t \in [0, 90]$ in Figure 9. This corresponds to 6186 time steps. Our numerical results show that the fully discrete energy remains constant up to $4e-14$ relative error.

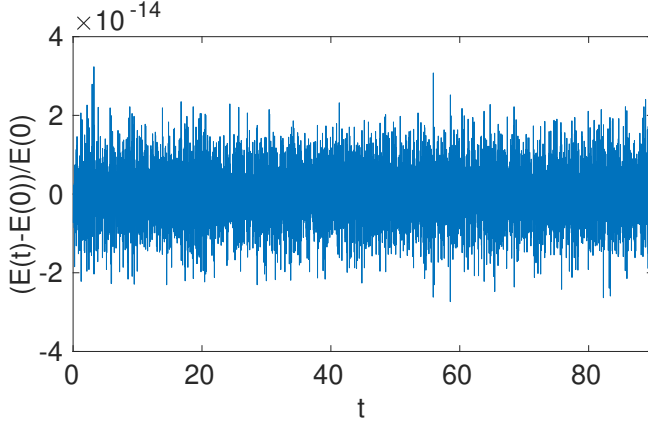


Figure 9: The relative change in fully discrete energy as a function of time. Here, $t = 90$ corresponds to 6186 time steps

6 Conclusion

A Appendix

$$P_1^T = \begin{pmatrix} 1 & 0 & 0 & 0 & 0 & 0 \\ 0 & 0 & 0 & 0 & 0 & 1 \\ 0 & 0 & 0 & 0 & 1 & 0 \end{pmatrix}, P_2^T = \begin{pmatrix} 0 & 0 & 0 & 0 & 0 & 1 \\ 0 & 1 & 0 & 0 & 0 & 0 \\ 0 & 0 & 0 & 1 & 0 & 0 \end{pmatrix}, P_3^T = \begin{pmatrix} 0 & 0 & 0 & 0 & 1 & 0 \\ 0 & 0 & 0 & 1 & 0 & 0 \\ 0 & 0 & 1 & 0 & 0 & 0 \end{pmatrix},$$

References

- [1] Kenneth Duru and Kristoffer Virta. Stable and high order accurate difference methods for the elastic wave equation in discontinuous media. *Journal of Computational Physics*, 279:37–62, 2014.
- [2] T. Hagstrom and G. Hagstrom. Grid stabilization of high-order one-sided differencing II: second-order wave equations. *J. Comput. Phys.*, 231:7907–7931, 2012.
- [3] H. O. Kreiss and J. Oliger. Comparison of accurate methods for the integration of hyperbolic equations. *Tellus*, 24:199–215, 1972.
- [4] Ken Mattsson and Jan Nordström. Summation by parts operators for finite difference approximations of second derivatives. *Journal of Computational Physics*, 199(2):503–540, 2004.
- [5] N Anders Petersson and Björn Sjögreen. Wave propagation in anisotropic elastic materials and curvilinear coordinates using a summation-by-parts finite difference method. *Journal of Computational Physics*, 299:820–841, 2015.
- [6] Björn Sjögreen and N Anders Petersson. A fourth order accurate finite difference scheme for the elastic wave equation in second order formulation. *Journal of Scientific Computing*, 52(1):17–48, 2012.
- [7] Joe F Thompson, Zahir UA Warsi, and C Wayne Mastin. *Numerical grid generation: foundations and applications*, volume 45. North-holland Amsterdam, 1985.

- [8] Siyang Wang and N Anders Petersson. Fourth order finite difference methods for the wave equation with mesh refinement interfaces. [arXiv preprint arXiv:1809.04310](https://arxiv.org/abs/1809.04310), 2018.